Inverse problem approach for SPHERE+ adaptive optics control

Clémentine Béchet, Michel Tallon, Eric Thiébaut, Isabelle Tallon-Bosc, Maud Langlois, Magali Loupias, Caroline Kulcsar, Henri Francois Raynaud, Nicolas Galland, I. Dinis, et al.

AO4ELT7 - June 2023 - Avignon

Inverse problem approach for SPHERE+ adaptive optics control

C. Béchet[a,b], M. Tallon[a], É. Thiébaut[a], I. Tallon-Bosc[a], M. Langlois[a], M. Loupias[a], C. Kulcsar[c], H.-F. Raynaud[c], N. Galland[c], I. Dinis[d], C. Goulas[e], F. Vidal[e], J. Milli[f], J. Mazoyer[e], R. Galicher[e], L. Schreiber[g], M. Feldt[h], A. Boccaletti[e], E. Diolaiti[g], G. Chauvin[i], F. Wildi[d], and R. Gratton[j]

[a]Univ. Lyon, Univ. Lyon1, Ens de Lyon, CNRS, Centre de Recherche Astrophysique de Lyon UMR5574, F-69230, Saint-Genis-Laval, France
[b]ANID - Millennium Nucleus for Applied Control and Inverse Problems (ACIP), Chile
[c]Université Paris-Saclay, Institut d'Optique Graduate School, CNRS, Laboratoire Charles Fabry, 91127 Palaiseau, France
[d]Observatoire de Geneve, CH-1290 Sauverny, Switzerland
[e]LESIA, Observatoire de Paris, Université PSL, Sorbonne Université, Université Paris Cité, CNRS, 5 place Jules Janssen, 92195 Meudon, France
[f]Univ. Grenoble Alpes, CNRS, IPAG, F-38000 Grenoble, France
[g]INAF - Osservatorio di Astrofisica e Scienza dello Spazio (OAS), 40129 Bologna, Italy
[h]Max-Planck-Institut fuer Astronomie, 69117 Heidelberg, Germany
[i]Laboratoire Lagrange, Université Cote d'Azur, CNRS, Observatoire de la Cote d'Azur, 06304 Nice, France
[j]INAF - Osservatorio Astronomico di Padova (OAPd), 35122 Padova, Italy

Further author information: (Send correspondence to C.B.)
C.B.: E-mail: clementine.bechet@univ-lyon1.fr

ABSTRACT

The SPHERE+ project is an upgrade of the high-contrast SPHERE instrument and of its adaptive optics (AO) named SAXO into SAXO+. SPHERE is currently installed at the Very Large Telescope in Chile. At the moment, SAXO uses a Shack-Hartmann wavefront sensor, a 41×41 deformable mirror (DM) and a tip-tilt mirror. SAXO+ will add a second stage with a near-infrared pyramid sensor and a second DM, to improve the contrast at low angular separation and to push further the limiting magnitude to work on fainter near-infrared targets. We present here the control method studied at the Centre de Recherche Astrophysique de Lyon (CRAL) for SAXO/SAXO+. This control relies on a global inverse problem approach and builds up on the THEMIS solar telescope AO control developed by the CRAL. Equations for the minimization of the global criterion lead to 2 optimizations steps: i) a wavefront estimation/prediction, ii) a projection on mirrors. Note that there is no classical integrator included in this CRAL control. Specific regularization choices are validated in presented simulations. In the first step, regularization for wavefront estimation is used with separated spatial and temporal penalty terms. We demonstrate: a) a high contrast performance in high flux conditions; b) that the temporal regularization improves performance in low flux conditions. In the second step, a regularization of the projection on mirrors is introduced based on a least-effort criterion. Concerning this step, we demonstrate that: a) the introduced concept of virtual piston mirror simplifies the optimization; b) we create an adjustable balance between mirrors for redundant modes (e.g. tip-tilt); c) this balance can be defined during design, independently on observing conditions. Although both steps are merged in THEMIS AO control real-time computer, we consider them separately for now in SAXO.

Keywords: control, optimization, high contrast, wavefront prediction, projection, regularization, stroke

1. INTRODUCTION

The SPHERE+ project is an upgrade of the high-contrast SPHERE instrument at the Very Large Telescope (VLT) in Chile. A key element of the project is the evolution of the current SAXO (SPHERE Adaptive eXtreme Optics) system installed there into a double-stage adaptive optics (AO) system, named SAXO Plus (SAXO+). SAXO+ aims at improving the contrast of the instrument at low angular separations and at pushing further the limiting magnitude to work on fainter near-infrared targets. SAXO currently uses a Shack-Hartmann wavefront sensor, a 41×41 high-order deformable mirror (HODM) and a tip-tilt (TT) mirror. SAXO+ will add a second stage with a pyramid wavefront sensor sensing in the near-infrared and an second DM, of type MEMS (micro electro-mechanichal system), will be added. The project also wants to demonstrate and compare advanced control methods on SAXO+ in the perspective of the future Planetary Camera and Spectrograph (PCS) on the Extremely Large Telescope (ELT).

We present here the first phase of the work done at the Centre de Recherche Astrophysiques de Lyon (CRAL) to study an advanced control for SAXO/SAXO+. This control relies on a global inverse problem approach and builds up on the AO control developed and installed by the CRAL on the THEMIS solar telescope [7]. The global approach allows to demonstrate that the control can be separated in two steps: i) the wavefront estimation problem and ii) the projection of the correction on mirrors (e.g. [5]). In THEMIS AO, there is only one wavefront sensor and one deformable mirror, and it has been chosen to gather the two steps in only one. To study SAXO+ control, we start considering the two steps separately having in mind that each one has to tackle a new feature:

- **wavefront estimation** must process data coming from sensors located at different stages and working at different frequencies
- **projection of the correction** must adequately distribute the efforts among several types of mirrors - high-order, tip-tilt, micro electro-mechanical mirrors (MEMS) mirror .

The work presented hereafter focuses on a preliminary phase, in which we extend the formalism developed for THEMIS AO control to the SAXO current design, in Sections 2 and 3. SAXO contains a high-order mirror and a tip-tilt mirror, which already requires addressing the projection of the correction among several mirrors, as mentioned above. The fusion of data coming from different sensors for the wavefront estimation remains the subject of further work. In Sec. 4, the performance of this control is analyzed with end-to-end simulations.

2. GLOBAL APPROACH EQUATIONS

For sake of clarity and consistency with practice, we consider a finite dimension representation of the wavefront in the pupil plane. The wavefront ϕ is defined as a combination of n_{wav} basis functions f_i of $\mathcal{L}_2(\mathbb{R}^2)$ such that

$$\phi(\boldsymbol{x}) = \sum_{i=1}^{n_{\text{wav}}} f_i(\boldsymbol{x})\, \boldsymbol{\phi}[i] \quad \forall \boldsymbol{x} \in \mathbb{R}^2\,. \tag{1}$$

We also introduce the semi-norm, $\|.\|_{\mathbf{W}_{\boldsymbol{A}}}$, defined over the pupil aperture such that for any wavefront ϕ by:

$$\|\phi\|^2_{\mathbf{W}_{\boldsymbol{A}}} = \boldsymbol{\phi}^{\mathrm{T}}\, \mathbf{W}_{\boldsymbol{A}}\, \boldsymbol{\phi} = \frac{\int_{\mathbb{R}^2} \sum_{i=1}^{n_{\text{wav}}} \sum_{j=1}^{n_{\text{wav}}} \boldsymbol{\phi}[i]\, \boldsymbol{\phi}[j]\, f_i(\boldsymbol{x}) f_j(\boldsymbol{x}) \mathcal{A}(\boldsymbol{x})\, \mathrm{d}\boldsymbol{x}}{\int_{\mathbb{R}^2} \mathcal{A}(\boldsymbol{x})\, \mathrm{d}\boldsymbol{x}} \tag{2}$$

with $\mathcal{A}(\boldsymbol{x})$ the masking aperture function with its value equal to 1 inside the aperture and 0 outside.

Considering a single wavefront sensor as in SAXO, at each time t when a new set of data $\boldsymbol{d}_t$ becomes available, we assume a linear model [7]

$$\boldsymbol{d}_t = \mathbf{S}\, \boldsymbol{\phi}_t + \boldsymbol{z}_t = \mathbf{S}\, (\boldsymbol{w}_t - \mathbf{M}\, \boldsymbol{a}_t) + \boldsymbol{z}_t \tag{3}$$

where $\mathbf{S} \in \mathbb{R}^{n_{\text{dat}} \times n_{\text{wav}}}$ represents the linearized SAXO sensor, $\boldsymbol{\phi}_t$ and $\boldsymbol{w}_t \in \mathbb{R}^{n_{\text{wav}}}$ represent respectively the residual and the incident wavefront during frame t, $\mathbf{M} = [\mathbf{M}_{\text{HO}}|\mathbf{M}_{\text{TT}}] \in \mathbb{R}^{n_{\text{wav}} \times n_{\text{act}}}$ stands for the influence matrix, $\boldsymbol{a}_t \in \mathbb{R}^{n_{\text{act}}}$ are the commands hold during frame t, and $\boldsymbol{z}_t \in \mathbb{R}^{n_{\text{dat}}}$ stands for the errors in the measurements of frame t. Here n_{dat} is the number of measurements per frame, n_{act} is the total number of mirrors degrees of freedom (or actuators). We note that the influence matrix $\mathbf{M}$ gathers the influence of all the mirrors, such that $\mathbf{M} = [\mathbf{M}_{\text{HO}}|\mathbf{M}_{\text{TT}}]$ with $\mathbf{M}_{\text{HO}}$ and $\mathbf{M}_{\text{TT}}$ the influence matrices of the high-order (HO) and tip-tilt (TT) mirrors respectively. The pseudo open-loop data associated to frame t can be written as

$$\boldsymbol{y}_t = \boldsymbol{d}_t + \mathbf{S}\, \mathbf{M}\, \boldsymbol{a}_t \tag{4}$$

such that the set of gathered information up to time t, noted $.|t$, consists in $\bigcup_{t' \leq t} \boldsymbol{y}_{t'}$.

2.1 A Piston-independent Criterion

Maximizing the Strehl ratio in AO corresponds to minimizing the mean-square piston-removed residual wavefront over the aperture,

$$\arg\min_{\boldsymbol{a}} \left\langle \|\mathbf{P} \cdot (\boldsymbol{w}_{t+\delta t} - \mathbf{M}\boldsymbol{a})\|^2_{\mathbf{W}_A} | t \right\rangle \tag{5}$$

where the subscript $t + \delta t$ is the instant when is applied the correction $\boldsymbol{a}$ deduced from the information gathered until time t, $\mathbf{P}$ is the piston-removal operator such that $\mathbf{P} \cdot \boldsymbol{\phi} := \boldsymbol{\phi} - \left(\mathbb{1}^{\mathrm{T}} \cdot \mathbf{W}_{\boldsymbol{A}} \cdot \boldsymbol{\phi}\right) \cdot \mathbb{1}$, with $\mathbb{1} = [1, 1, \ldots, 1]^{\mathrm{T}}$, and $\langle \cdots | t \rangle$ denotes expectation knowing gathered information up to time t.

This criterion is just a particular case of the formalism presented in [2], with only on-axis correction to be optimized. This allows us to simplify the criterion considering the residual piston as an additional component to the model. For this, a virtual piston mirror of unique degree of freedom (single command a_p) is added into the influence matrix model $\mathbf{M}$ of Eq. (3), such that now $\mathbf{M} = [\mathbf{M}_{\text{HO}}|\mathbf{M}_{\text{TT}}|\mathbf{M}_{\text{P}}]$. $\mathbf{M}_{\text{P}}$ is able to produce any piston that would be required to best fit the wavefront $\boldsymbol{w}_{t+\delta t}$, even if the high-order mirrors cannot. This enhance the generality of the present work, which does not require any null-piston assumption on the wavefront $\boldsymbol{w}$.

With this augmented influence matrix, the piston removal operator is no longer needed and the AO optimization problem simplifies to:

$$\arg\min_{\boldsymbol{a}} \left\langle \|\boldsymbol{w}_{t+\delta t} - \mathbf{M}\boldsymbol{a}\|^2_{\mathbf{W}_A} | t \right\rangle\,. \tag{6}$$

2.2 From a Global Criterion to two Separated Steps

Developing the quadratic form of the criterion of Eq. (6) leads to

$$\boldsymbol{a}_{t+\delta t} = \arg\min_{a} \left[\left\langle \|\boldsymbol{w}_{t+\delta t}\|^2_{\mathbf{W}_A} | t \right\rangle - 2 \left\langle \boldsymbol{w}_{t+\delta t} | t \right\rangle^{\mathrm{T}} \mathbf{W}_{\boldsymbol{A}} \mathbf{M}\, \boldsymbol{a} + \boldsymbol{a}^{\mathrm{T}} \mathbf{M}^{\mathrm{T}} \mathbf{W}_{\boldsymbol{A}} \mathbf{M}\, \boldsymbol{a} \right] \tag{7}$$

So, $\boldsymbol{a}_{t+\delta t}$ is solution of the minimization if

$$\mathbf{M}^{\mathrm{T}} \mathbf{W}_{\boldsymbol{A}} \mathbf{M}\, \boldsymbol{a}_{t+\delta t} = \mathbf{M}^{\mathrm{T}} \mathbf{W}_{\boldsymbol{A}} \left\langle \boldsymbol{w}_{t+\delta t} | t \right\rangle = \mathbf{M}^{\mathrm{T}} \mathbf{W}_{\boldsymbol{A}}\, \boldsymbol{w}_{t+\delta t|t}\,. \tag{8}$$

where we simplify the notations in the last right hand side to write the expected value knowing the information up to a given time t, *i.e.* $\boldsymbol{w}_{t+\delta t|t} = \langle \boldsymbol{w}_{t+\delta t} | t \rangle$. As already noticed in [7], Eq. (8) reveals that only the statistics, not the actual realization, of the future wavefront need to be known. To estimate $\boldsymbol{w}_{t+\delta t|t}$, all the equations developed in sections 2.1 to 2.4 in [7] apply here. It is out of the scope of this paper to reproduce all the equations and the reader is encouraged to see [7] for the mathematical details. We however remind hereafter the updating rules that are derived there:

$$\boldsymbol{w}_{t'|t} = \boldsymbol{w}_{t'|t-1} + \mathbf{C}_{\boldsymbol{w}_{t'},\boldsymbol{w}_t|t-1}\, \mathbf{C}^{-1}_{\boldsymbol{w}_t|t-1} \left(\boldsymbol{w}_{t|t} - \boldsymbol{w}_{t|t-1} \right) \ \forall\, t'\,, \tag{9}$$

$$\text{in particular} \quad \boldsymbol{w}_{t+\delta t|t} = \boldsymbol{w}_{t+\delta t|t-1} + \mathbf{C}_{\boldsymbol{w}_{t+\delta t},\boldsymbol{w}_t|t-1}\, \mathbf{C}^{-1}_{\boldsymbol{w}_t|t-1} \left(\boldsymbol{w}_{t|t} - \boldsymbol{w}_{t|t-1} \right)\,, \tag{10}$$

$$\text{with} \quad \boldsymbol{w}_{t|t} = \boldsymbol{w}_{t|t-1} + \left(\mathbf{S}^{\mathrm{T}}\, \mathbf{C}^{-1}_{\boldsymbol{z}_t}\, \mathbf{S} + \mathbf{C}^{-1}_{\boldsymbol{w}_t|t-1} \right)^{-1} \mathbf{S}^{\mathrm{T}}\, \mathbf{C}^{-1}_{\boldsymbol{z}_t} \left(\boldsymbol{y}_t - \mathbf{S}\, \boldsymbol{w}_{t|t-1} \right) \tag{11}$$

$$\text{and} \quad \mathbf{C}^{-1}_{\boldsymbol{w}_t|t} = \mathbf{C}^{-1}_{\boldsymbol{w}_t|t-1} + \mathbf{S}^{\mathrm{T}}\, \mathbf{C}^{-1}_{\boldsymbol{z}_t} \cdot \mathbf{S}\,. \tag{12}$$

Note that the notations $\mathbf{C}_{\boldsymbol{x}|t}$ and $\mathbf{C}_{\boldsymbol{x},\boldsymbol{x}'|t}$ stand respectively for the covariance of vector $\boldsymbol{x}$ with itself, and of vector $\boldsymbol{x}$ with vector $\boldsymbol{x}'$, knowing the gathered information up to time t. The right part of Eq. (10) evidences that solving equation Eq. (11) is required each time t a new data vector becomes available.

The control therefore consists in computing two successive steps:

1. the wavefront estimation of $\boldsymbol{w}_{t+\delta t|t}$ which involves a Maximum *A Posteriori* (MAP) estimation of $\boldsymbol{w}_{t|t}$ defined in Eq. (11),
2. the projection of the estimate on the mirrors to deduce the best commands $\boldsymbol{a}_{t+\delta t}$ by solving the system of normal equations in Eq. (8).

The implementation of each of these two steps is analyzed in Sec. 3.

3. CONTROL STEPS APPROXIMATIONS FOR REAL-TIME

Although we have obtained expressions and updating rules for an optimal estimate of the wavefront at every new frame, we do not have yet a rule to update the temporal cross-covariances in Eqs. (10)-(11) at every step. It is also necessary to minimize the latency of the AO control computation. All these constraints have led to approximate the estimation step by another estimator detailed in the present section. Such approximations are inspired from what has been implemented in THEMIS AO system.

3.1 Regularized Wavefront Estimation

As a first simplification, the best prediction of the incoming wavefront at time $t + \delta t$, $\boldsymbol{w}_{t+\delta t|t}$, is assumed to simply be the MAP estimate of the wavefront at time t, $\boldsymbol{w}_{t|t}$. We then consider

$$\boldsymbol{w}_{t+\delta t|t} \simeq \boldsymbol{w}_{t|t} = \left(\mathbf{S}^{\mathrm{T}}\, \mathbf{C}^{-1}_{\boldsymbol{z}_t}\, \mathbf{S} + \mathbf{C}^{-1}_{\boldsymbol{w}_t|t-1} \right)^{-1} \left(\mathbf{S}^{\mathrm{T}}\, \mathbf{C}^{-1}_{\boldsymbol{z}_t}\, \boldsymbol{y}_t + \mathbf{C}^{-1}_{\boldsymbol{w}_t|t-1}\, \boldsymbol{w}_{t|t-1} \right)\,, \tag{13}$$

where we have just factorized Eq. (11) using the fact that $\mathbf{I} = (\mathbf{S}^{\mathrm{T}}\, \mathbf{C}^{-1}_{\boldsymbol{z}_t}\, \mathbf{S} + \mathbf{C}^{-1}_{\boldsymbol{w}_t|t-1})^{-1} (\mathbf{S}^{\mathrm{T}}\, \mathbf{C}^{-1}_{\boldsymbol{z}_t}\, \mathbf{S} + \mathbf{C}^{-1}_{\boldsymbol{w}_t|t-1})$. It is then interesting to notice that Eq. (13) is equivalent to solving the minimization problem

$$\boldsymbol{w}_{t|t} = \arg\min_{\boldsymbol{w}} \|\mathbf{S}\, \boldsymbol{w} - \boldsymbol{y}_t\|^2_{\mathbf{C}^{-1}_{\boldsymbol{z}_t}} + \|\boldsymbol{w} - \boldsymbol{w}_{t|t-1}\|^2_{\mathbf{C}^{-1}_{\boldsymbol{w}_t|t-1}} \tag{14}$$

It is not straightforward to compute in real time an estimate of the spatio-temporal covariance $\mathbf{C}_{\boldsymbol{w}_t|t-1}$. We have thus chosen for the moment to approximate the spatio-temporal regularization term in Eq. (14) by two separate regularizations, a spatial one applied with a scalar weight μ_t and a temporal one applied with a scalar weight ρ_t. We thus write the approximate regularization as

$$\|\boldsymbol{w} - \boldsymbol{w}_{t|t-1}\|^2_{\mathbf{C}^{-1}_{\boldsymbol{w}_t|t-1}} \simeq \mu_t \, \|\boldsymbol{w}\|^2_{\mathbf{C}^{-1}} + \rho_t \, \|\boldsymbol{w} - \boldsymbol{w}_{t-1|t-1}\|^2_{\mathbf{W}_{\boldsymbol{A}}} \tag{15}$$

where $\mathbf{C}$ is the fractal approximation of the von Karman turbulence wavefront covariance[6, 1]. Therefore the estimate of the wavefront at time t becomes

$$\boldsymbol{w}_{t|t} = \arg\min_{\boldsymbol{w}} \, \|\mathbf{S} \cdot \boldsymbol{w} - \boldsymbol{d}_t - \mathbf{S}\,\mathbf{M}\,\boldsymbol{a}_t\|^2_{\mathbf{C}^{-1}_{\boldsymbol{z}_t}} + \mu_t \, \|\boldsymbol{w}\|^2_{\mathbf{C}^{-1}} + \rho_t \, \|\boldsymbol{w} - \boldsymbol{w}_{t-1|t-1}\|^2_{\mathbf{W}_{\boldsymbol{A}}} \tag{16}$$

In practice, until now on SAXO simulations, we have only a static approximation of the noise covariance matrix $\mathbf{C}^{-1}_{\boldsymbol{z}_t} = \mathbf{C}^{-1}_{\boldsymbol{z}}$, $\forall t$, which is a normalized weighting matrix defined by the percentage of illumination of each subaperture. We also use static values for $\mu_t = \mu$ and $\rho_t = \rho$ (*i.e.* independently of time t).

The exact equation solved in SAXO simulations so far for the wavefront estimation is then written as

$$\boldsymbol{w}_{t+\delta t|t} \simeq \boldsymbol{w}_{t|t} = \left(\mathbf{S}^{\mathrm{T}}\,\mathbf{C}^{-1}_{\boldsymbol{z}}\,\mathbf{S} + \mu\,\mathbf{C}^{-1} + \rho\mathbf{I}\right)^{-1} \left(\mathbf{S}^{\mathrm{T}}\,\mathbf{C}^{-1}_{\boldsymbol{z}}\,\boldsymbol{y}_t + \rho\boldsymbol{w}_{t-1|t-1}\right) . \tag{17}$$

or equivalently

$$\boldsymbol{w}_{t+\delta t|t} \simeq \boldsymbol{w}_{t|t} = \left(\mathbf{S}^{\mathrm{T}}\,\mathbf{C}^{-1}_{\boldsymbol{z}}\,\mathbf{S} + \mu\,\mathbf{C}^{-1} + \rho\mathbf{I}\right)^{-1} \left[\mathbf{S}^{\mathrm{T}}\,\mathbf{C}^{-1}_{\boldsymbol{z}}\,(\boldsymbol{d}_t + \mathbf{S}\,\mathbf{M}\,\boldsymbol{a}_t) + \rho\boldsymbol{w}_{t-1|t-1}\right] . \tag{18}$$

3.2 Regularized Projection on Mirrors

The second step of the control is now to solve (see Eq. (8))

$$\mathbf{M}^{\mathrm{T}}\,\mathbf{W}_{\boldsymbol{A}}\,\mathbf{M} \cdot \boldsymbol{a}_{t+\delta t|t} = \mathbf{M}^{\mathrm{T}}\,\mathbf{W}_{\boldsymbol{A}} \cdot \boldsymbol{w}_{t|t} \, . \tag{19}$$

The issue about solving equation (19) is that there may exist an infinity of solutions $\boldsymbol{a}_{t+\delta t|t}$, because $\mathbf{M}^{\mathrm{T}}\,\mathbf{W}_{\boldsymbol{A}}\,\mathbf{M}$ is usually singular. There can be redundant modes between different mirrors range spaces and there may also be unseen actuators in the pupil aperture. At least, there are probably badly seen actuators on the edges, making the system of equations ill-conditioned. This is why regularization should be introduced in the optimization. We distinguish here two kinds of regularizations (not exclusive):

A. effort-based regularization

B. uncertainty-based regularization (acting on badly seen modes)

In the work presented here, we have only implemented the latter and it was enough to obtain a stable AO control behavior in the SAXO simulations.

We describe here in more details the way this regularization is inserted. Such kind of regularization has already been used by [4] and aims at expressing the effort associated to each actuator control. Typically, a tip-tilt correction may be as well produced by the HO DM or by a dedicated tip-tilt mirror. However, we prefer to use the tip-tilt mirror as much as we could, so we can weight the tip-tilt command vector part $\boldsymbol{a}_{TT}$ to favor its use. For this, we introduce a diagonal regularization term as follows in the projection criterion

$$\boldsymbol{a}_{t+\delta t|t} = \arg\min_{a} \, \|\boldsymbol{w}_{t|t} - \mathbf{M}\boldsymbol{a}\|^2_{\mathbf{W}_A} + \mu_d \, \|\mathbf{D}\,\boldsymbol{a}\|^2_2 \, . \tag{20}$$

where $\mathbf{D}$ is a diagonal matrix and μ_d is a scalar hyperparameter to weight the regularization level. The regularized solution is simply obtained as

$$\boldsymbol{a}_{t+\delta t|t} = \left(\mathbf{M}^{\mathrm{T}}\,\mathbf{W}_{\boldsymbol{A}}\,\mathbf{M} + \mu_d\,\mathbf{D}^{\mathrm{T}}\,\mathbf{D}\right)\mathbf{M}^{\mathrm{T}}\,\mathbf{W}_{\boldsymbol{A}} \cdot \boldsymbol{w}_{t|t} \, . \tag{21}$$

To favor redundant modes to be produced by a given mirror rather than by another, it is sufficient to use 3 non-zero scalar values α_{HO}, α_{TT} and α_{P} to build $\mathbf{D}$ as a diagonal matrix with $\mathbf{D}_{i,i} = 1/\alpha_{\mathrm{HO}}^2$ for all i among the HO mirror degrees of freedom, $\mathbf{D}_{i,i} = 1/\alpha_{\mathrm{TT}}^2$ for i indexes corresponding to tip and tilt and $\mathbf{D}_{i,i} = 1/\alpha_{\mathrm{P}}^2$ for the virtual piston. This leads to solve

$$\boldsymbol{a}_{t+\delta t|t} = \arg\min_{a} \|\boldsymbol{w}_{t|t} - \mathbf{M}\boldsymbol{a}\|_{\mathbf{W}_A}^2 + \frac{\mu_d}{\alpha_{\mathrm{HO}}^2}\|\boldsymbol{a}_{\mathrm{HO}}\|_2^2 + \frac{\mu_d}{\alpha_{\mathrm{TT}}^2}\|\boldsymbol{a}_{\mathrm{TT}}\|_2^2 + \frac{\mu_d}{\alpha_{\mathrm{P}}^2}\|\boldsymbol{a}_{\mathrm{P}}\|_2^2 . \tag{22}$$

The important benefits of this regularized optimization approach are:

- As soon as all diagonal terms of $\mathbf{D}$ are non-zero, $\boldsymbol{a}_{t+\delta t|t}$ is uniquely defined
- When $\mu_d \to 0^+$, the criterion tends towards the same minimum value as Eq. (6)
- If μ_d is chosen *small enough* the correction error $\|\boldsymbol{w}_{t|t} - \mathbf{M}\boldsymbol{a}_{t+\delta t|t}\|_{\mathbf{W}_A}^2$ is also minimal
- Taking α_{TT} and α_{P} large enough (compared to α_{HO}) favors correcting the tip-tilt and the piston mostly via $\boldsymbol{a}_{\mathrm{TT}}$ and $\boldsymbol{a}_{\mathrm{P}}$, that is not via the HO DM.

The effect of α values on the projection is demonstrated in simulations in Sec. 4.4.

4. SIMULATIONS RESULTS

In this section, we assess the performance of the presented controller using end-to-end simulations of SAXO/SAXO+. The simulations are run with COMPASS [8], which is selected in the SAXO+ project to be the common platform to run end-to-end simulations. It is possible to simulate either the first stage only (SAXO) or both stages of the AO (SAXO+). The main parameters used for the simulations are detailed in Sec. 4.1. In Sec. 4.2, the best achievable performance of the controller is first analyzed using a high-flux case and median atmospheric conditions. This allows to check the behavior of the controller in conditions where we expect the hardware design to be the limiting factor (number of actuators, maximum frequency). Next, the controller is tested in low-flux conditions in Sec. 4.3, meaning that the ability of the controller to face large measurement errors is analyzed. Last, more specific simulation of correction of a dummy wavefront is used to demonstrate the potential benefit of the proposed equations for the projection on mirrors in Sec. 4.4.

The project has a reference controller for each, SAXO first stage only and SAXO+ double-stage system. They both rely on matrix-vector multiplications using a truncated basis of Karhunen-Loeve modal representation of the system projected on the mirrors space, and classical integrator controllers [3]. In comparison, the controller developed in Sec. 2 is applied on the first stage (SAXO only) so far. It relies on Eqs. (18) and (22) and does not contain any classical integral controller. It is referred as CRAL controller in the presentation of the simulations results hereafter.

4.1 SAXO/SAXO+ Simulations Parameters

The SAXO stage (i.e. first stage) simulates the 40×40 Shack-Hartmann wavefront sensor, with a square spatial filter of size $1.5\lambda/d$ ($d = 20$ cm, $\lambda = 700$ nm). A detector noise of $0.1\mathrm{e}^-$/pixel/frame is simulated. The second stage simulation part includes a near-infrared ($\lambda = 1.2$ μm) Pyramid wavefront sensor with 50 pixels across the diameter of each pupil image on the sensor detector. The pyramid modulation is set to $3\lambda/D$ ($D = 8$ m). The first stage frequency is set to the current maximum frequency used in SAXO system at Paranal, 1380 Hz. The second stage is simulated at twice this frequency (2760 Hz). The exact factor two between both stages frequencies is for the moment chosen as a reference since it accelerates the simulations. This may evolve during the SAXO+ project. The HODM of SAXO is simulated with its 1377 actuators. The tip-tilt mirror is simulated in the first stage. A MEMS deformable mirror with 28×28 actuators is simulated for the second stage.

The simulation of the atmosphere is made using a 35-layer profile, with a seeing of 0.5 arcseconds. The coherence time of the simulated atmosphere is equal to 3 ms.

COMPASS allows to simulate 5-second long exposures with AO correction, with and without a perfect coronograph. It also provides the achieved photon-limited contrast curves [3]. A long-exposure Strehl ratio is also assessed at $\lambda = 1650$ nm.

For the reference controllers, the integrator default gain value is 0.3 (in high flux conditions), SAXO stage is controlled using 1200 modes and the second stage adds 400 more modes to the correction.

4.2 High Flux Results

The first simulations aim at testing that our approximation in the MAP wavefront estimate (see Eq.(18)) allows to control SAXO stage with high performance in high-flux conditions. This correspond to the simulations conditions considered in the SAXO+ project as the "science case 1", simulating the guide star brightness as follows: G mag= 5.5 for SAXO stage and H mag= 5.1 for SAXO+ stage [9]. Such bright case leads to an average number of 307 photons/subaperture/frame on the Shack-Hartmann and 21 photons/pixel/frame for the second stage sensor.

The obtained photon-limited contrast curves are shown in Fig. 1. Since there are no non-common path aberrations included so far in the simulations, the depth of these contrast curves is the more important criterion to determine the AO performance.

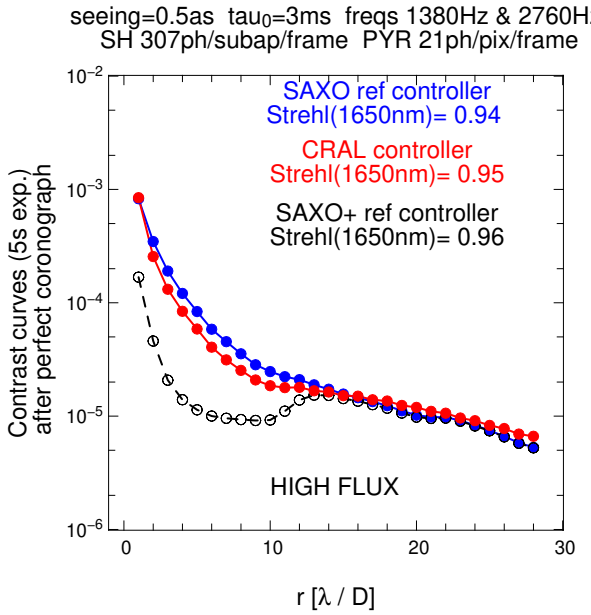

Figure 1. SAXO+ Science case 1. Simulation results (exposure time: 5 seconds) with CRAL controller (red) on SAXO stage, reference controller (blue) on SAXO stage and reference controller (black) on SAXO+ double-stage AO.

We observe that the proposed controller (red) in high flux conditions provides similar or better contrast than the reference one applied on SAXO stage (blue). It can be even noticed an improved contrast at low separation angles. However, a larger range of simulations in different atmospheric conditions are required to quantitatively analyze this contrast performance at low separations. It can be noticed that the contrast improvement provided by the addition of the SAXO+ second stage (black curve) is much larger (a factor 5 to 10 in intensity).

These results evidence the fact that the proposed controller efficiently corrects the atmospheric turbulence down to what the design of SAXO stage allows with its 1377 actuators and a maximum frequency of 1380Hz.

4.3 Low Flux Results

In low flux conditions, the measurement errors increase and the wavefront estimation is more difficult. So far, COMPASS simulations only provide the measured slopes without the uncertainty level on each measurement,

so a static precision matrix approximation $\mathbf{C}_z$ is used in the WF estimate of Eq. (18). Still the amplitude of diagonal elements of $\mathbf{C}_z$ increases at lower flux. Some temporal control like a classical integrator for the reference controller, or the temporal regularization with $\rho > 0$ in Eq. (18) are expected to mitigate the noise propagation in the AO correction due to this loss of flux. Figure 2 presents the contrast curves (left graph) obtained for SAXO in low flux conditions (average of 3 photons/frame/subaperture on the Shack-Hartmann sensor).

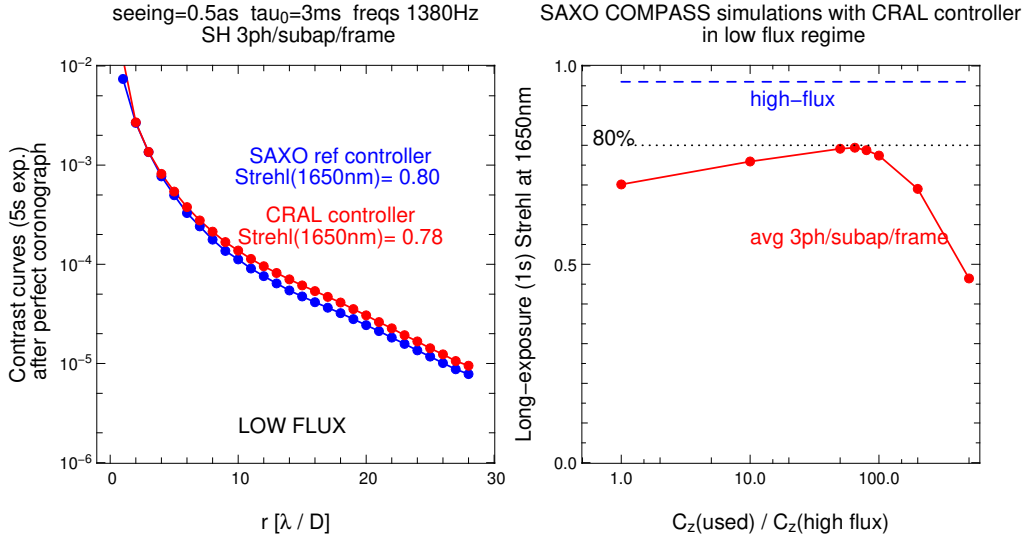

Figure 2. Left: Same simulation case and controls of SAXO as in Fig. 1 but at low flux (average of 3 photons/frame/subaperture on the Shack-Hartmann). The reference controller integrator gain has been lowered to 0.2 to face the noise increase. Right: Long-Exposure Strehl ratio (at 1650 nm) *vs* assumed noise value $\mathbf{C}_z$ for the MAP wavefront estimation in Eq. (18). The left graph red contrast curve has been obtained with the best $\mathbf{C}_z$ estimate in this right graph. Dash blue horizontal line stands as a reference of the high flux Strehl ratio.

The two controllers achieve similar Strehl ratio values (80% for the reference controller, 78% for the proposed controller) and similar contrast curves. In order to optimize the reference controller performance at low flux the integrator gain has been changed to 0.2. The CRAL controller has no integrator, but the increase of the covariance of the measurement noise $\mathbf{C}_z$ must be taken into account in the equations to optimize the correction. The right part of the Fig. 2 evidence the fact if the change in the noise covariance is not taken into account (i.e. $\mathbf{C}_z(\text{used})/\mathbf{C}_z(\text{high flux}) = 1$, the Strehl ratio would drop down to 70%. An overestimation of the noise covariance is not good either. There is, as expected, an optimal correction with 80% Strehl ratio obtained when the increase of the measurement error is well estimated.

As already mentioned, the measurements coming from COMPASS simulations do not come with precision information. A future work consists in the implementation of the errors covariance estimation from the Shack-Hartmann centroiding computation at every frame, as is the case in the real-time computer of THEMIS AO.

4.4 Balanced Projection Between Mirrors

The last simulations presented here illustrate the way Eq. (22) allows to balance the effort asked to each mirror in order to obtain the best correction of a given wavefront. For this, a dummy perturbed wavefront is created from the addition of a cosine perturbation, a piston and a tilt over a square area of 40×40 (in units of actuators pitch). The wavefront must be optimally corrected by the combination of a piston (virtual) mirror, a tip-tilt mirror and a HODM mirror, over a circular aperture of diameter $D = 36$ (in units of actuator pitch). This is the wavefront goal for which 1D-cuts taken at the center of the pupil is shown in magenta on the graphs of Fig. 3.

Applying the projection step described by Eq. (22), we can deduce what is the correction contribution assigned to each of the mirrors. The result depends on the values of the regularization hyperparameters α_{HO}, α_{TT} and α_{P}. On the left, all the hyperparameters are set to equal value, and this tends to distribute the piston and tilt among

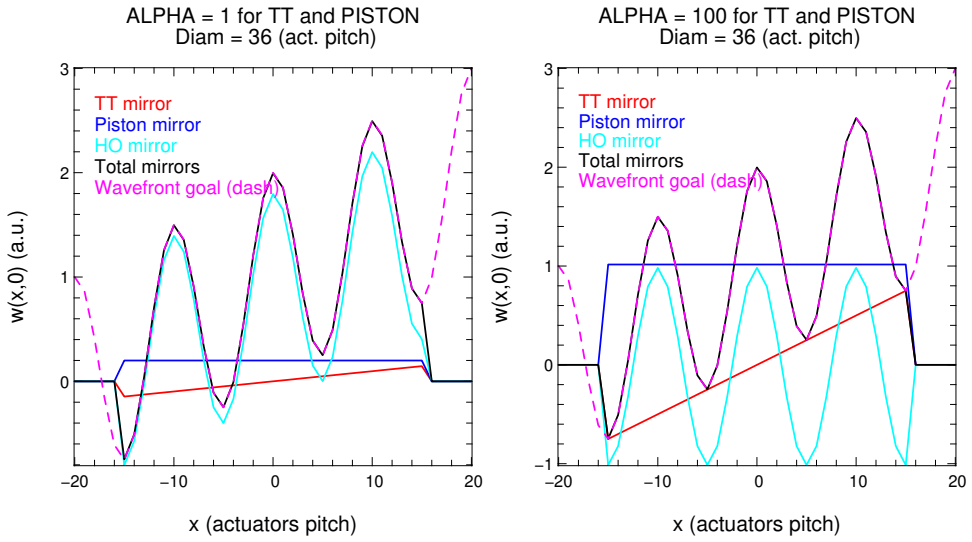

Figure 3. Results of projections of a dummy wavefront containing a cosine wave, a piston and a tilt, onto a system modeled using $\mathbf{M} = [\mathbf{M}_{\mathrm{HO}}|\mathbf{M}_{\mathrm{TT}}|\mathbf{M}_{\mathrm{P}}]$. Contributions of each mirror: piston (blue), TT (red) and HODM (cyan) are presented, as well as their total (additive correction). Left: with $\alpha_{\mathrm{TT}} = \alpha_{\mathrm{P}} = 1$. Right: with $\alpha_{\mathrm{TT}} = \alpha_{\mathrm{P}} = 100$. In both cases, $\alpha_{\mathrm{HO}} = 1$, $\mu_d = 10^{-7}$.

the several mirrors that can produce it. We see for instance that the HODM contribution contains a tilt part, and also a non-zero piston. The TT mirror only corrects for a small portion of the tilt contained in the goal correction. On the contrary, setting by RTC design the hyperparameters of the equation to $\alpha_{\mathrm{HO}} = 1$ and $\alpha_{\mathrm{P}} = \alpha_{\mathrm{TT}} = 100$, allows to almost completely exclude the piston and tilt contributions from the HODM correction. This is key to save the stroke of the HODM in a multiple-mirror system. It is also interesting to see how the virtual piston $\mathbf{M}_{\mathrm{P}}$ included in the model allows to avoid a bias in the correction, with an impact equivalent to having previously removed the piston from the wavefront estimate or from the system modes.

5. CONCLUSION

The inverse problem approach is used to study at CRAL an adaptive optics control algorithm for the upgrade of the SAXO system into SAXO+. This work builds upon the success of THEMIS solar adaptive optics system, also developed and implemented by the CRAL. The formalism is derived so far for the first stage, SAXO. We have obtained a 2-step control method, with the usual separation of: 1) wavefront estimation and 2) projection on the mirrors. The specificity of the proposed control relies on the choices made to approximate the optimization solutions in each step. For the wavefront estimation step, so far no prediction is made but the MAP estimate is modified to include 2 separate regularizations: i) spatial regularization and ii) temporal regularization. For the projection step, the regularization allows to adequately balance the efforts between the mirrors and to save the HODM stroke.

The performance of this control method is demonstrated using end-to-end simulations of the SAXO systems on COMPASS. Beyond providing the same performance as the reference controller in high flux conditions, we also demonstrate that the temporal regularization included in the WF estimation is as efficient as a classical integrator control to face the increase of the measurements noise in median atmospheric conditions.

The controller needs to be further developed to account for the fusion of data coming from both stages of SAXO+, if the project maintains the perspective of an integrated AO architecture for the two stages.

ACKNOWLEDGMENTS

The authors also acknowledge CNRS/INSU support of the SAXO+ project. Clémentine Béchet acknowledges Chilean funding of Millennium Nucleus for Applied Control and Inverse Problems, through the grant ANID-MILENIO-NCN19_161.

References

[1] C. Béchet, M. Tallon, and É. Thiébaut. "Comparison of minimum-norm maximum likelihood and maximum a posteriori wavefront reconstructions for large adaptive optics systems". In: *J. Opt. Soc. Am. A* 26.3 (2009), pp. 497–508.

[2] E. Brunner, C. Béchet, and M. Tallon. "Optimal projection of reconstructed layers onto deformable mirrors with fractal iterative method for AO tomography". In: *Adaptive Optics Systems III*. Vol. 8447. Proc. SPIE. 2012, p. 84475I.

[3] C. Goulas et al. "SAXO Plus upgrade: second stage adaptive optics system end-to-end numerical simulations". In: *in this conference*. Vol. VII. AO4ELT. 2023.

[4] C. Kulcsár et al. "Minimum variance control in presence of actuator saturation in adaptive optics". In: *Adaptive Optics Systems*. Vol. 7015. Proc. SPIE. 2008, 70151G.

[5] C. Petit et al. "Linear quadratic Gaussian control for adaptive optics and multiconjugate adaptive optics: experimental and numerical analysis". In: *J. Opt. Soc. Am. A* 26.6 (2009), pp. 1307–1325.

[6] É. Thiébaut and M. Tallon. "Fast minimum variance wavefront reconstruction for extremely large telescopes". In: *J. Opt. Soc. Am. A* 27.5 (2010), pp. 1046–1059.

[7] É. Thiébaut et al. "Closing the loop as an inverse problem: the real-time control of THEMIS adaptive optics". In: *Adaptive Optics Systems VIII*. Vol. 12185. Proc. SPIE. 2022.

[8] F. Ferreira et al. "Numerical estimation of wavefront error breakdown in adaptive optics". In: *Astronomy & Astrophysics* 616 (2018), A102.

[9] M. Langlois et al. "Science test cases benchmark: simulations towards SPHERE Plus high contrast performances". In: *in this conference*. Vol. VII. AO4ELT. 2023.